Purdue University
Purdue e-Pubs

Other Nanotechnology Publications   Birck Nanotechnology Center

8-28-2009

Strain energy and lateral friction force distributions of carbon nanotubes manipulated into shapes by atomic force microscopy

Mark C. Strus
Purdue Unversity, mark.strus@nist.gov

Roya R. Lahiji
Purdue University, lahiji@ualberta.ca

Pablo Ares
Nanotec Electronica

Vincente Lopez
Universidad Autonoma de Madrid

Arvind Raman
Purdue University, raman@purdue.edu

See next page for additional authors

Follow this and additional works at: http://docs.lib.purdue.edu/nanodocs

Part of the Applied Mechanics Commons, Engineering Physics Commons, Nanoscience and Nanotechnology Commons, Other Materials Science and Engineering Commons, and the Other Mechanical Engineering Commons

Authors

Mark C. Strus, Roya R. Lahiji, Pablo Ares, Vincente Lopez, Arvind Raman, and Ron R. Reifenberger

Strain energy and lateral friction force distributions of carbon nanotubes manipulated into shapes by atomic force microscopy

Mark C Strus[1,2,6]**, Roya R Lahiji**[1,3]**, Pablo Ares**[4]**, Vicente López**[5]**, Arvind Raman**[1,2] **and Ron Reifenberger**[1,3]

[1] Birck Nanotechnology Center, Purdue University, West Lafayette, IN, USA
[2] School of Mechanical Engineering, Purdue University, West Lafayette, IN, USA
[3] Department of Physics, Purdue University, West Lafayette, IN, USA
[4] Nanotec Electronica, Madrid, Spain
[5] Universidad Autonoma de Madrid, Madrid, Spain

E-mail: mark.strus@nist.gov

Abstract

The interplay between local mechanical strain energy and lateral frictional forces determines the shape of carbon nanotubes on substrates. In turn, because of its nanometer-size diameter, the shape of a carbon nanotube strongly influences its local electronic, chemical, and mechanical properties. Few, if any, methods exist for resolving the strain energy and static frictional forces along the length of a deformed nanotube supported on a substrate. We present a method using nonlinear elastic rod theory in which we compute the flexural strain energy and static frictional forces along the length of single walled carbon nanotubes (SWCNTs) manipulated into various shapes on a clean SiO_2 substrate. Using only high resolution atomic force microscopy images of curved single walled nanotubes, we estimate flexural strain energy distributions on the order of attojoules per nanometer and the static frictional forces between a SWCNT and SiO_2 surface to be a minimum of 230 pN nm^{-1}.

(Some figures in this article are in colour only in the electronic version)

1. Introduction

The unique electrical, chemical, and mechanical properties [1] of single walled carbon nanotubes (SWCNTs) [2] make them promising candidates for many device applications in nanotechnology such as nanocircuits [3], chemical sensors [4], mass transport carriers [5], and nanorelays [6]. In many cases, the electrical and chemical properties of SWCNTs strongly depend on their mechanical deformations. For example, both chemical reactivity [7] and radical-binding strength [8] of SWCNTs tend to increase as local strain energy is enhanced by CNT bending. Electrical properties of SWCNTs have been shown to be uniquely coupled to their mechanical properties [9] and highly reversible even at large deformations [10].

The inherent structural flexibility of carbon nanotubes (CNTs) provides many potential advantages in advanced nanoscale electromechanical applications due to the novel electromechanical coupling and the potential solution to strain relief and routing agility not possible with more conventional interconnects. In future CNT-based circuit applications [11], the band structure of the SWCNT will be fined-tuned by adjusting the flexural strain energy [12]. Because chemical reactivity is related to local strain, the sensitivity of CNTs used for chemical sensors will likely increase by simply optimizing their shape. In spite of the important connection between shape and function in CNTs, little is quantitatively known about the flexural strain energies and friction forces that hold a CNT in a particular shape.

---

[6] Author to whom any correspondence should be addressed.

1

When an electrically neutral SWCNT is deposited on a substrate, surface forces, that are ultimately related to van der Waals interactions between the underlying surface and the supported CNT, cause an adhesion of the SWCNT to the substrate. Surface roughness [13], nanotube–substrate atomic composition/commensurability [14], and the presence of intervening molecular adlayers all play important roles in modulating the adhesive force. If the SWCNT is then elastically deformed by some external force such as an atomic force microscope probe, strain energy will be stored in the bent CNT. If the lateral interaction forces between the CNT and the substrate are sufficiently weak, the stored elastic energy is released as the internal shear forces and bending moments cause the CNT to spring back to its original shape. If the net lateral forces between the CNT and the substrate are sufficiently high, it is possible that the CNT may maintain its deformed shape on the substrate. Such lateral forces may arise from van der Waals or chemical interactions between the nanotube and the substrate or from CNT pinning due to catalyst particles on the substrate. To date, little is known about the magnitude of the lateral frictional forces that develop and no general approach has been presented to study these forces in a systematic way.

In what follows we demonstrate that atomic force microscopy (AFM) manipulation of carbon nanotubes provides one way to investigate strain energies and static friction forces between SWCNTs and SiO$_2$ surfaces. AFM manipulation has been proposed as a method of fabricating prototypical CNT-based nanodevices [15–21], because AFM-based techniques are capable of physically deforming and subsequently imaging carbon nanotubes. While most AFM manipulation studies have investigated localized buckling of CNTs [15–17], their intrinsic elastic strain energies and lateral force distributions have been overlooked, despite their influence on the electrical and chemical properties.

In this work, we describe a convenient method using only high resolution AFM topographical images of SWCNTs manipulated into different shapes on a surface to infer the local strain energy distribution of lateral frictional forces acting on curved SWCNTs as a function of length. We present a series of AFM manipulation experiments to demonstrate the capabilities of the strain energy lateral force (SELF) algorithms we have developed to map out the stored flexural strain energy and static friction forces required to maintain the final shape of the SWCNT and a SiO$_2$ surface. We also systematically discuss the various sources of error encountered when using the method. While the technique is developed for a particular materials system, it is completely general and can be used to learn more about the stored strain energies and lateral surface forces for a wide variety of different nanowire–substrate systems.

2. Experiments

In order to conduct the studies described below, it was important to disperse SWCNTs on a flat, clean substrate. Deposition of CNTs dispersed in a liquid solvent was rejected because the evaporation of the liquid will inevitably leave

behind a contamination layer on the underlying substrate. The method chosen was to grow individual SWCNTs on a flat substrate using chemical vapor deposition (CVD) techniques.

A 200 nm thick silicon oxide SiO$_2$ layer was thermally grown on a p-type 15 Ω cm Si ⟨100⟩ wafer at 800 °C in air and cooled down to room temperature. The SWCNT catalyst was deposited by spin-coating 20 μl of 0.46 mM 2-propanol solution of Fe(NO$_3$)$_3$9H$_2$O followed by rinsing for 2 s in n-hexane followed by drying it under a stream of argon gas. The catalyst and substrate were then introduced into a CVD reactor with a constant flow pressure of 200 sccm of H$_2$ and 800 sccm of Ar at 850 °C for 15 min to ensure the complete reduction of iron. Subsequently, the conditions were readjusted by keeping constant the flows of H$_2$ and Ar and adding to this mixture 2.5 sccm of ethylene and 50 sccm of H$_2$O/Ar to avoid the amorphous carbon formation, for 6 min. Finally, the flow of Ar at 200 sccm was maintained while cooling the substrate to room temperature.

The Si substrates were then imaged using noncontact AFM and found to contain both SWCNTs dispersed across a flat substrate and a few remaining catalyst particles. None of the SWCNTs tested in this study were initially attached to the surface via their catalyst particles, though it was possible for the CNTs to interact with catalyst particles during their manipulation. Based on roughness calculations of areas of the SiO$_2$ surface without CNTs or catalyst particles, the root mean square roughness (RMS) was found to be 6 Å [22]. The value of the RMS roughness also matched closely with the average roughness calculated from the topography scans of the SiO$_2$ substrate. In addition, the statistical distribution of the surface topography was well described by a Gaussian profile. Taken together, all these indicators indicate the SiO$_2$ substrate is smooth and devoid of large hills and/or pits, suggesting that the lateral frictional forces can be reasonably approximated as uniform across the surface, except when the CNT encounters a catalyst particle.

Isolated SWCNTs were located with a Nanotec Electronica™ atomic force microscope operating under ambient conditions with ≈30% relative humidity. Olympus OMCL-AC240TS-C2™ microcantilevers with nominal spring constants of 1.8 N m^{-1} were used to first image isolated SWCNTs via attractive regime amplitude-modulated mode imaging [23], thus insuring the CNTs are not deformed by the microcantilever tip. The WSxM software [24] lithography option was used to manipulate the 265 nm long SWCNT, shown in figure 1, into eight different shapes. In each manipulation, the AFM tip was dragged across the surface in a 200–300 nm straight line while operating in contact mode with a constant normal force, typically, at least 50 nN. After manipulation, attractive regime amplitude-modulated AFM was again used to image the CNTs.

The tip undergoes considerable tip wear when operating in contact mode for manipulation, thus explaining the large apparent lateral dimension of the CNT in figure 1. Nonetheless, the CNT centerline can be well resolved based on choosing a line halfway between the inner and outer edges of the image, and subsequently near the highest *z*-height in the cross section (see figure 1 cross-section inset) [25]. By the application
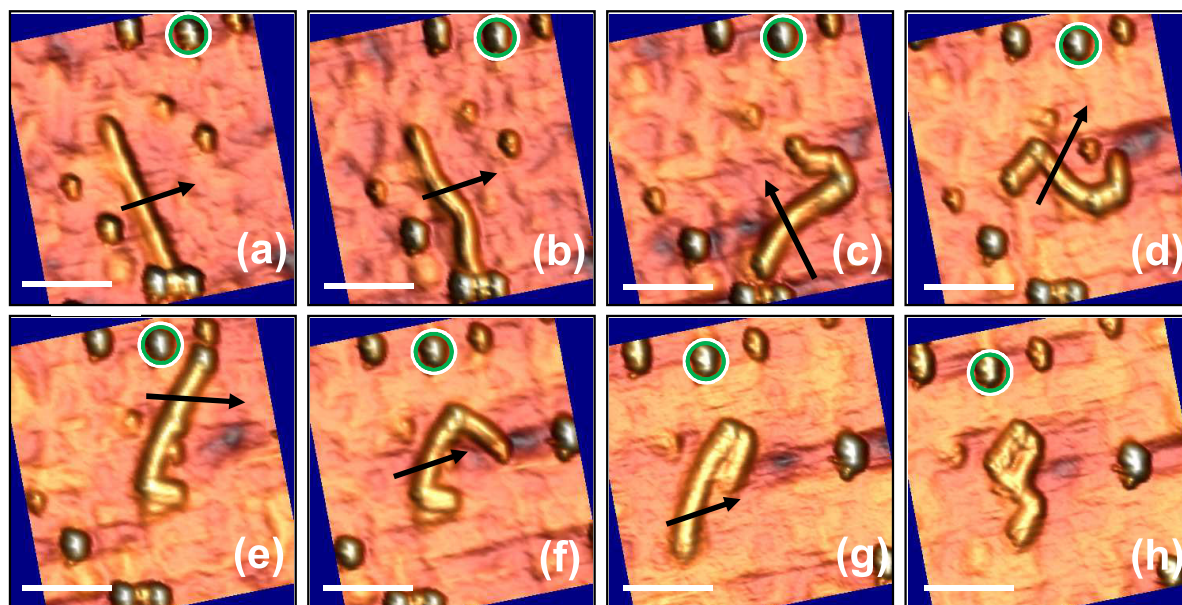
Figure 1. Noncontact AFM images obtained with WSxM [24] showing a series of eight manipulations (a)–(h) on the same SWCNT using AFM contact mode. Each black arrow shows the direction of manipulation leading to the subsequent CNT shapes. The manipulation starts with (a) a straight SWCNT that it is eventually manipulated into (h) a 'P' shape. During some of the manipulations the CNT partially returns to its undeformed shape indicating all manipulations are highly elastic processes. The green circle with outer white circle is a reference to the same sample location (a leftover catalyst particle) in each scan. The white scale bar represents 80 nm. The SWCNT is 265 nm in length with average diameter of 1.6 nm (based on average AFM height measurements—see figure 2).

of smoothing techniques, the random errors can be reduced, though such errors can still be significant especially near points of high curvature.

The SWCNT in figure 1(a) was initially straight, then subsequently manipulated into the shapes shown in figures 1(a)–(h) leading to a final structure resembling the letter 'P' (figure 1(h)). The arrows in each image represent the direction the AFM tip was dragged across the surface in contact mode, thus deforming the CNT into each subsequent shape. Based on the average height of the undeformed tube in figure 1(a), the CNT had an average outer diameter of 1.6 nm. In its deformed configurations, the CNT diameter did vary, particularly near areas of largest curvature, where some local buckling may have occurred. When CNTs buckle, their shell collapses releasing energy as the CNT cross section switches into a different morphological pattern [26]. However, it is hard to prescribe local buckling as the only source of this height change since it is also possible that the CNT is locally pinned by a catalyst particle.

3. Model and analysis

Simulations have shown that carbon nanotubes are remarkably resilient, sustaining extreme elastic strain with no signs of brittleness, plasticity, or atomic rearrangements [26]. Thus, continuum mechanical approximations have been useful in quantitatively predicting large flexural deformations of long CNTs [26, 27], such as those studied in this work. Furthermore, because CNTs typically have small diameters and large axial elastic modulus, the strain energy due to applied loads is dominated by flexural strain energy in comparison

to axial strain energy[7], such that an Euler elastica rod model [28, 29] can be employed to approximate strain energy and lateral force distributions of carbon nanotubes [30–33]. In contrast to common Bernoulli–Euler models, which are applicable only for infinitesimal deformations, elastica rod models are applicable when significant bending is present.

The proposed method assumes that CNT slopes and curvatures vary smoothly and that no local buckling occurs. If there are a discrete number of points where the CNT buckles locally, then the proposed method can be extended piecewise to compute the strain energies and lateral forces to each smooth section of the CNT, while neglecting strain energy contributions at the local buckles. In what follows, we outline the general method, which can be applied either to the entire CNT or to the smooth sections of the CNT if the local buckling points are known *a priori*.

The goal of the SELF method is to first obtain the *x* and *y* Cartesian positions of each point along the length of the CNT curve, parameterize these so that every point can be written as a function of the arc displacement *s*, and then define the CNT curve in localized tangential–normal coordinates that vary with *s* so that the curvature can be calculated. Figure 2(a) shows a noncontact AFM topographical scan of the same SWCNT in figure 1 bent into an 'S' shape. Overlaid on top of the SWCNT image are a series of data points capturing the centerline location of the SWCNT. The Cartesian coordinate

---

[7] If one assumes a SWCNT with $d = 1.6$ nm, $L_{CNT} = 265$ nm, $E = 1$ GPa, and $t = 0.34$ nm, then the ratio of the axial stiffness, $k_a = EA/L_{CNT}$, (A is cross-sectional area) to bending stiffness ($k_b = EI/L_{CNT}^3$) is nearly 10^5, such that the CNT will be much more likely to bend than axially stretch.
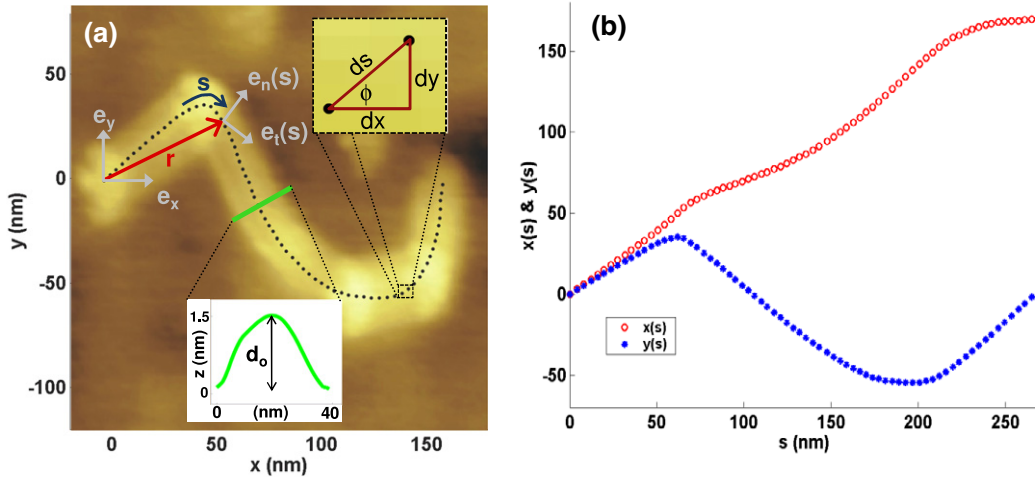
Figure 2. (a) AFM topography image of a SWCNT manipulated into an 'S' shape where the data points of the CNT centerline have been obtained using a program such as DataThief [34]. Each point is converted from $\mathbf{r} = x\mathbf{e_x} + y\mathbf{e_y}$ coordinates to $\mathbf{r}(s) = x(s)\mathbf{e_x} + y(s)\mathbf{e_y}$ using the geometric relationship shown in the inset, where $x(s)$ and $y(s)$ are shown in (b). The width of the CNT looks large in the two-dimensional topography because a fairly blunt tip was used in noncontact mode to obtain the image. However, the accurate CNT diameter of the CNT can still be calculated from maximum height of the cross-sectional profile of the CNT shown by the inset.

$\mathbf{r} = x\mathbf{e_x} + y\mathbf{e_y}$ of each centerline point[8] was captured by eye using DataThief software [34] though more sophisticated tracing algorithms could also be used [25, 35]. The measured differences, dx and dy, between successive points on the curve with respect to the $\mathbf{e_x}$ and $\mathbf{e_y}$ unit vectors are calculated and used to find the change in the arc displacement ds using the known geometrical relationship, $ds^2 = dx^2 + dy^2$ (see the inset in figure 2(a)). As a result, each point of the CNT centerline can be described by

$$\mathbf{r}(s) = x(s)\mathbf{e_x} + y(s)\mathbf{e_y}, \qquad (1)$$

where $x(s)$ and $y(s)$ are shown in figure 2(b). In order to calculate the strain energy of the SWCNT along its length, the local curvature, $\rho(s)$ (where $R = 1/\rho(s)$ is the radius of curvature), is first calculated from Frenet–Serret formulae for a space curve [36]. Each point on the SWCNT curve is converted to a tangential–normal coordinate system as shown by unit vectors $\mathbf{e_t}(s)$ and $\mathbf{e_n}(s)$ in figure 2(a), such that

$$\mathbf{e_t}(s) = \frac{d\mathbf{r}}{ds}(s) = \frac{dx}{ds}(s)\mathbf{e_x} + \frac{dy}{ds}(s)\mathbf{e_y}, \qquad (2)$$

and

$$\mathbf{e_n}(s) = \frac{d\mathbf{e_t}}{ds}(s) \bigg/ \left| \frac{d\mathbf{e_t}}{ds}(s) \right|$$
$$= \frac{1}{\rho(s)} \left(\frac{d^2 x}{ds^2}(s)\mathbf{e_x} + \frac{d^2 y}{ds^2}(s)\mathbf{e_y} \right). \qquad (3)$$

Thus, the curvature is derived directly from the magnitude of the tangential unit vector such that

$$\frac{d\phi}{ds}(s) = \frac{1}{\rho(s)} = \sqrt{\left(\frac{d^2 x}{ds^2}(s) \right)^2 + \left(\frac{d^2 y}{ds^2}(s) \right)^2}. \qquad (4)$$

[8] DataThief software [34] extracts the coordinates of the CNT centerline, which has been defined visually by choosing the line halfway between the inner and outer edges of the image, and subsequently near the highest z-height in the cross section. For best results while calculating higher derivatives, points were captured every 30–40 nm along the length of the CNT.

Here $\phi(s)$ is the angle that the vector ds makes with the horizontal as indicated in figure 2(a). The $x(s)$ and $y(s)$ derivatives in equations (2) and (3) have been calculated numerically using the secant method with minimal smoothing using either three- or five-point running mean averages[9]. With the curvature known along the length of the CNT, the strain energy distribution per unit length is readily calculated from

$$U_s(s) = \frac{EI}{2} \left(\frac{d\phi}{ds}(s) \right)^2, \qquad (5)$$

where E is the bending elastic modulus of the CNT and I is the area moment such that $I = \frac{\pi}{8} d_o^3 t$, where d_o is the outer diameter of the CNT, and $t = 0.34$ nm is the assumed SWCNT wall thickness [37]. For a given CNT shape, the total strain energy, U_T in the tube is found by integrating the strain energy distribution along the length of the tube, such that

$$U_T = \int_0^{L_{CNT}} \frac{EI}{2} \left(\frac{d\phi}{ds}(s) \right)^2 ds. \qquad (6)$$

[9] $E(s)$ and $F_n(s)$ were obtained through several numerical derivatives using the secant method, which, as a high pass filter, magnifies small variations in collected data, which are much smaller than the possible true curvatures. Hence, three- and five-point running mean average filters were used to smooth the data after each derivative to eliminate these derivative artifacts. To assess the validity of the SELF algorithms, several well-defined polynomial curves were generated similar the $x(s)$ and $y(s)$ curves defined for each SWCNT shape. Based on these curves and their analytically defined derivatives, hypothetical $E(s)$ and $F_n(s)$ functions were calculated as a benchmark to estimate the error in the numerically based SELF method. The SELF method was applied to plots of $x(s)$ and $y(s)$ such that $E(s)$ and $F_n(s)$ could be found. The error between each numerically generated point and analytically calculated benchmark curves was calculated separately for $E(s)$ and $F_n(s)$, resulting in Gaussian distributions of the respective errors. Based on several generated polynomial benchmark examples derived from the actual SWNCT shapes in figure 1, the largest standard deviations of the error-based Gaussian distributions have been reported as the errors for calculating $E(s)$ and $F_n(s)$. Because errors tend to be largest at the ends of the SWCNT where differentiation and smoothing are most difficult due to lack of data points, errors have also been reported for cases where a number of end points are ignored.
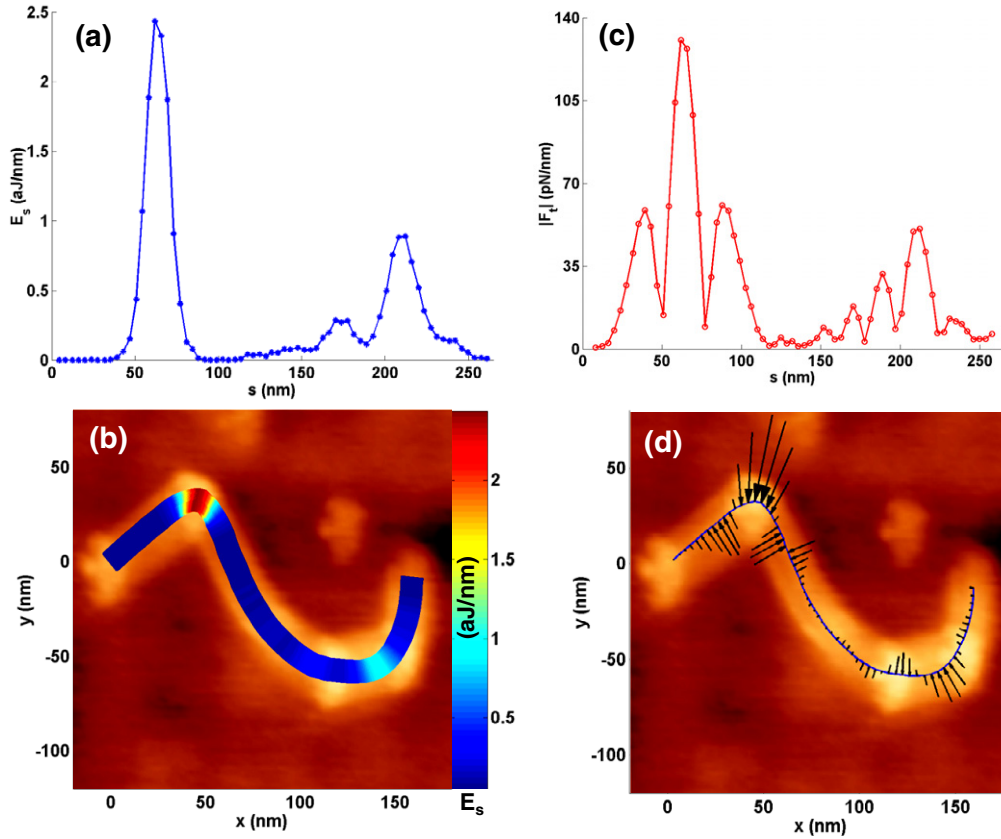
Figure 3. (a) The strain energy distributions along the length of a SWCNT manipulated into a 'S' shape show strains on the order of attojoules per nanometer, while (b) visually demonstrates where largest strain occurs in the SWCNT. (c) Friction force distributions along the length of the 'S' SWCNT are on the order of 100 pN nm^{-1}, where (d) shows where the frictional forces act on the deformed CNT to prevent it from returning to its undeformed position. The arrows in (d) have been normalized by the maximum frictional force per unit length.

Assuming the contribution to the lateral frictional force due to axial stretching is small, the lateral frictional force, $F_n(s)$, can be calculated from force and moment equilibrium balance considerations. It is easy to show that the lateral frictional force as a function of s required to maintain an elastically deformed CNT shape is related to the third derivative of ϕ such that

$$F_n(s) = -EI\frac{\mathrm{d}^3\phi}{\mathrm{d}s^3}(s)\mathbf{e_n}. \qquad (7)$$

4. Results

Typical strain energy distributions and frictional forces computed using the SELF algorithm above for a 'S' shape SWCNT are shown in figure 3, assuming $E = 1$ TPa [38]. As shown in figure 3(a), strain energies are largest near greatest curvature, reaching a maximum of 2.4 aJ nm^{-1}. Assuming E and I are well defined and no localized buckling, strain energy distribution is estimated to be within ± 0.2 aJ nm^{-1} of the true value near the center of the CNT and within ± 1.1 aJ nm^{-1} near the beginning and ends of the SWCNT where differentiation and smoothing is most difficult due to lack of data points (see footnote 9). These errors are from finite point secant method differentiation and subsequent smoothing and tend to underpredict the total strain energy (see footnote 9), particularly near regions of high curvature.

The total strain energy for each deformed CNT shape has been shown in table 1. Because E and I are assumed constant, the shape of the CNT (number of bends and degree of bending angles) determines the differing strain energies in the entire CNT. Without accurate knowledge of the strain energy distribution throughout the CNT length, it could be difficult to determine which shape led to a higher value of total strain energy in the CNT. Such measurements could be pivotal for the design of nanoelectrical circuits with bent SWCNTs, where the total CNT resistance depends on the total strain energy. In addition to total strain energy, table 1 shows the maximum tensile strain, $\epsilon_{\max} = \frac{d_o}{2\rho}$, for each SWCNT shape in figure 1.

Once the stored strain energy is calculated, the lateral frictional forces between the 'S' shape SWCNT and SiO$_2$ can be estimated by applying equation (7). The magnitude of this lateral force applied by the substrate to the nanotube is plotted in figure 3(c) as a function of position along the nanotube. Due to fourth order numerical differentiation involved in the extraction of these quantities, these values are believed to be well within ± 72 pN nm^{-1} of true values near the center of the SWCNTs (assuming E and I are well defined and no local buckling) and within ± 150 pN nm^{-1} at the ends of the SWCNT (see footnote 9). Because of numerical differentiation errors, the sum of the friction forces in the x and y direction are not zero as expected, but finite (≈ 1 nN). The lateral forces

Table 1. The minimum radius of curvature $R = 1/\rho$ and corresponding maximum strain energy U_s (indicated by arrows) as well as the total strain energy U_T, maximum tensile strain ϵ_{max}, and maximum frictional force F_n of the manipulated SWCNT for each shape (a)–(h) in figure 1. The CNT was assumed to have an elastic modulus $E = 1$ TPa [38] and average diameter of 1.6 nm (see figure 2).

CNT shape								
R (nm)	390	40	24	17	20	15	18	16
U_s (aJ nm^{-1})	0.0038	0.25	0.55	1.2	0.8	1.6	0.9	1.5
U_T (aJ)	0.16	6.6	28	38	17	44	36	71
ϵ_{max} (%)	0.20	2.0	3.3	4.7	3.9	5.3	4.4	5.1
F_n (pN nm^{-1})	4.0	36	61	130	94	230	51	130

for the 'S' shape SWCNT in figure 3 are found to reach a maximum of 130 ± 72 pN nm^{-1} in the region of the nanotube with the smallest radius of curvature [25, 39]. Since the shape of the nanotube is stable, the lateral static frictional force between the 'S' shape SWCNT and SiO$_2$ substrate must be greater than this value.

Surprisingly, lateral frictional forces act along the entire length of the SWCNT as indicated in figure 3(d), some intuitively in directions that maintain the bent SWCNT shape, and others surprisingly in directions that would return the CNT to an undeformed shape. Nonetheless, the net sum of the lateral friction forces must keep the SWCNT balanced and immobilized in its deformed shape. The maximum frictional forces found for each CNT configuration are reported in table 1 and reach a maximum value of 230 ± 72 pN nm^{-1} for the 'U' shaped SWCNT in figure 1(f), setting a useful lower limit for the lateral static frictional forces between a SWCNT and SiO$_2$ substrate.

5. Sources of error

In many of the CNT shapes analyzed (table 1) the maximum lateral forces, which occur at points of maximum curvature, are rather large. The associated lateral shear stresses approach hundreds of megapascals which could be indicative of local buckling. In this case, the SELF algorithm should be deployed piecewise to sections of the curve that exclude the buckling point in a similar manner to what has been already described. However, in practice, it is hard to be certain that local buckling did in fact occur at these points for the following reasons: (a) one does not know the critical lateral stress required for local buckling without rigorously modeling of the CNT such as with molecular dynamics simulations [27], and (b) the high lateral forces could also arise from interactions between the CNTs and isolated catalyst particles fixed on the substrate. Thus, we conclude that the SELF algorithm can also be used, in conjunction with appropriate modeling efforts, to identify points where the CNTs buckle locally. If such points are identified positively, then the strain energy and lateral force distributions need to be recalculated by applying the SELF algorithm, piecewise, to sections of the CNT, excluding the buckling points.

It is worthwhile discussing the systematic and random uncertainties associated with the SELF algorithm when applied to smooth sections of the CNT. The CNT is subject to systematic (offset tip radius) and random (variable tip roughness) errors. Systematic errors will lead to an offset image, but will have no affect on the calculated curvature. Random errors due to sub-nanometer tip roughness are likely to be most critical near areas of large curvature. However, these random errors are essentially eliminated by the applied smoothing techniques.

Care must also be exercised when tracing the coordinates of the nanostructure through a small radius of curvature. For small radii of curvature, coordinate measurement errors may skew the results more than the random errors described previously. For a small radius of curvature ($\approx$20 nm), frictional errors on the order of 100 pN nm^{-1} can result unless sophisticated tracing algorithms [25, 35] are employed, which can pinpoint the planar coordinates of the bent nanostructure to a high degree of accuracy.

6. Conclusions

AFM images of CNTs and nanowires on substrates are routinely taken for the characterization of electrochemical or chemimechanical materials and devices. We show in this paper that AFM images of the curved shape of a CNT on a substrate reveal a wealth of information on the strain energies and lateral forces on the CNT, thus boosting the information that can be gathered from AFM images of CNTs and other nanowires. The AFM's ability to locally manipulate and subsequently image deformed CNTs was coupled with a systematic continuum elastic model to estimate strain energies. The developed strain energy lateral force (SELF) algorithms allowed us to map out the stored flexural strain energy, extract the lateral surface forces required to maintain the final shape of a SWCNT on an SiO$_2$ substrate, and identify possible buckling points along the CNT.

Additionally, the ability to estimate frictional force gradients offers insight about the surface forces required to maintain a CNT in a particular deformed position. The surface force gradients measured in this way not only reflect the interaction force between a CNT and a particular substrate but also the modification of these forces by molecular adsorbates. It is now possible to evaluate the relative strength of these two contributions in a systematic way by utilizing the SELF algorithm coupled with controlled manipulation experiments on nanowires supported by a variety of chemically different substrates.

The SELF algorithm, being based on image analysis, comes with its sources of error, of which the three principal ones are (a) the presence of local buckling, which if confirmed by appropriate models, requires the SELF algorithm to be adjusted and applied piecewise to non-buckled sections of the CNT, (b) systematic errors in tracing the centerline of the CNT which lead to minimal effects on the strain energy and lateral force measurements, and (c) random errors in tracing the centerline which can lead to significant errors especially near regions of high curvature. These sources of error must be carefully taken into account while applying the algorithm to AFM images.

Acknowledgments

References

[1] Saito R, Fujita M, Dressellhaud G and Dresselhaus M S 1998 *Physical Properties of Carbon Nanotubes* (London: Imperial College Press)

[2] Iijima S 1991 Helical microtubules of graphitic carbon *Nature* **354** 56–8

[3] Chen Z H, Appenzeller J, Lin Y M, Sippel-Oakley J, Rinzler A G, Tan J Y, Wind S J, Solomon P M and Avouris P 2006 An integrated logic circuit assembled on a single carbon nanotube *Science* **311** 1735

[4] Kong J, Franklin N R, Zhou C, Chapline M G, Peng S, Cho K and Dai H 2000 Nanotube molecular wires as chemical sensors *Science* **287** 622–5

[5] Regan B C, Aloni S, Ritchie R O, Dahmen U and Zettl A 2004 Carbon nanotubes as nanoscale mass conveyors *Science* **428** 924–7

[6] Jang J E, Cha S N, Choi Y, Amaratunga G A J, Kang D J, Hasko D G, Jung J E and Kim J M 2005 Nanoelectromechanical switches with vertically aligned carbon nanotubes *Appl. Phys. Lett.* **87** 163114

[7] Park S, Srivstava D and Cho K 2003 Generalized chemical reactivity of curved surfaces: carbon nanotubes *Nano Lett.* **3** 1273–7

[8] Mylvganam K and Zhang L C 2006 Deformation-promoted reactivity of single-walled carbon nanotubes *Nanotechnology* **17** 410–4

[9] Postma H W C, Teepen T, Yao Z, Grifoni M and Dekker C 2001 Carbon nanotube single-electron transistors at room temperature *Science* **293** 76–9

[10] Tombler T W, Zhou C, Alexseyev L, Kong J, Dai H, Liu L, Jyanthi C S, Tang M and Wu S-Y 2000 Reversible electromechanical characteristics of carbon nanotubes under local-probe manipulation *Nature* **405** 769–72

[11] Avouris P, Hertel T, Martel R, Schmidt T, Shea H R and Walkup R E 1999 Carbon nanotubes: nanomechanics, manipulation, and electronic devices *Appl. Surf. Sci.* **141** 201–9

[12] Minot E D, Yaish Y, Sazonova V, Park J-Y, Brink M and McEuen P L 2003 Tuning carbon nanotube band gaps with strain *Phys. Rev. Lett.* **90** 156401

[13] Delrio F W, de Boer M P, Knapp J A, Reedy E D Jr, Clews P J and Dunn M L 2005 The role of van der Waals forces in adhesion of micromachined surfaces *Nature* **5** 629–34

[14] Falvo M R, Steele J, Taylor R M II and Superfine R 2000 Evidence of commensurate contact and rolling motion: AFM manipulation studies of carbon nanotubes on HOPG *Tribol. Lett.* **9** 73–6

[15] Falvo M R, Clary G J, Taylor R M II, Chi V, Brooks F P Jr, Washburn S and Superfine R 1997 Bending and buckling of carbon nanotubes under large strain *Nature* **389** 582–4

[16] Postma H W C, Sellmeijer A and Dekker C 2000 Manipulation and imaging of individual single-walled carbon nanotubes with an atomic force microscope *Adv. Mater.* **12** 1299–302

[17] Duan X, Tang C, Zhang J, Guo W and Liu Z 2007 Two distinct buckling modes in carbon nanotube bending *Nano Lett.* **7** 143–8

[18] Hertel T, Martel R and Avouris P 1998 Manipulation of individual carbon nanotubes and their interaction with surfaces *J. Phys. Chem.* B **102** 910–5

[19] Decossas S, Patrone L, Bonnot A M, Comin F, Derivaz M, Barski A and Chevrier J 2003 Nanomanipulation by atomic force microscopy of carbon nanotubes on a nanostructured surface *Surf. Sci.* **543** 57–62

[20] Falvo M R, Taylor R M II, Helser A, Chi V, Brooks F P Jr, Washburn S and Superfine R 1999 Nanometre-scale rolling and sliding of carbon nanotubes *Nature* **397** 236–8

[21] Kashiwase Y, Ikeda T, Oya T and Ogino T 2008 Manipulation and soldering of carbon nanotubes using atomic force microscope *Appl. Surf. Sci.* **253** 7897–900

[22] Bennett J and Mattsson L 1989 *Introduction to Surface Roughness and Scattering* (Washington, DC: Optical Soceity of America)

[23] Garcìa R and San Paulo A 1999 Attractive and repulsive tip–sample interaction regimes in tapping-mode atomic force microscopy *Phys. Rev.* B **60** 4961–7

[24] Horcas I, Fernández R, Gómez-Rodríguez J M, Colchero J, Gómez-Herrero J and Baro A M 2007 WSxM: a software for scanning probe microscopy and a tool for nanotechnology *Rev. Sci. Instrum.* **78** 013705

[25] Conache G, Gray S M, Ribayrol A, Fröberg L E, Samuelson L, Pettersson H and Montelius L 2009 Friction measurements of InAs nanowires on silicon nitride by AFM manipulation *Small* **4** 203–7

[26] Yakobson B I, Brebec C J and Bernholc J 1996 Nanomechanics of carbon tubes: instabilities beyond linear response *Phys. Rev. Lett.* **76** 2511–4

[27] Pantano A, Parks D M and Boyce M C 2004 Mechanics of deformation of single- and multi-wall carbon nanotubes *J. Mech. Phys. Solids* **52** 789–821

[28] Love A E H 1944 *A Treatise on the Mathematical Theory of Elasticity* (New York: Dover)

[29] Frisch-Fray R 1962 *Flexible Bars* (Washington, DC: Butterworth)

[30] Oyharcabal X and Frisch T 1999 Peeling off an elastic from a smooth attractive substrate *Phys. Rev.* E **71** 036611

[31] Strus M C, Zalamea L, Raman A, Pipes R B, Nguyen C V and Stach E A 2008 Peeling force spectroscopy: exposing the adhesive nanomechanics of one-dimensional nanostructures *Nano Lett.* **8** 544–50

[32] Lee S I, Howell S W, Raman A, Reifenberger R, Nguyen C V and Meyyappan M 2004 Nonlinear tapping dynamics of multi-walled carbon nanotube tipped atomic force microcantilevers *Nanotechnology* **15** 416–21

[33] Strus M C, Cano C, Pipes R B, Nguyen C V and Raman A 2009 Interfacial energy measurements between carbon nanotubes

and select polymers through the use of peeling force spectroscopy *Compos. Sci. Technol.* **69** 1580–6

[34] Tummers B 2006 *Datathief III* http://datathief.org/ Datathief is a program used to reverse engineer data points from a graph

[35] Wiggins P A, van der Heijden T, Moreno-Herrero F, Spakowitz A, Phillips R, Widom J, Dekker C and Nelson P C 2006 High flexibility of DNA on short length scales probed by atomic force microscopy *Nat. Nanotechnol.* **1** 137–41

[36] do Carmo M P 1976 *Differential Geometry of Curves and Surfaces* (Englewood Cliff, NJ: Prentice-Hall)

[37] Wang Q and Varadan V K 2005 Stability analysis of carbon nanotubes via continuum models *Smart Mater. Struct.* **14** 281–6

[38] Wang C Y and Zhang L C 2008 A critical assessment of the elastic properties and effective wall thickness of single-walled carbon nanotubes *Nanotechnology* **19** 075705

[39] Bordag M, Ribayrol A, Conache G, Fröberg L E, Gray S, Samuelson L, Montelius L and Pettersson H 2007 Shear stress measurements on InAs nanowires by AFM manipulation *Small* **3** 1398–401